



The effect of wash treatment on the mechanical properties and energy absorption potential of a 3D printed polymethyl methacrylate (PMMA)

Alexander Bardelcik^{a,*}, Steven Yang^a, Faraz Alderson^{a,b}, Andrew Gadsden^a

^a School of Engineering, College of Engineering and Physical Sciences, University of Guelph, 50 Stone Road East, N1G 2W1, Guelph, Ontario, Canada

^b Virox Technologies Incorporated, 2770 Coventry Road, L6H 6R1, Oakville, Ontario, Canada

ARTICLE INFO

Keywords:

Stereolithography 3D printing
Polymethyl methacrylate (PMMA)
Wash treatment
Tensile testing
Mechanical properties
Finite element analysis
Octet-truss lattice structure

ABSTRACT

Stereolithographic 3D-printing of a Polymethyl Methacrylate (PMMA) resin was used to manufacture miniature dog-bone specimens that were subject to a variety of wash treatments consisting of Isopropyl Alcohol (IP), Hydrogen Peroxide (HP) and a Detergent (D) solution. The washed dog-bone specimens were then tested in uniaxial tension and the mechanical properties were quantified to assess the potential use of the resultant materials for the design of energy absorbing lattice structures. Compared to an As-Printed material, a detergent wash treatment resulted in almost no loss in peak stress, but a 61 % increase in toughness due to enhanced elongation. Moderate decreases in peak stress and high elongation were observed for HP washes. A 5 % (concentration) HP wash with detergent (HP5 + D) resulted in a 90 % greater toughness than the As-Printed material. Isopropyl washed specimens showed low toughness due to low peak stresses. A finite element study was conducted to simulate compression tests of an octet-truss lattice structure for which the tensile test properties were used as model inputs. The simulations revealed some relationships between the predicted energy absorption-tensile properties and showed that the HP5 + D (moderate peak force) and As-Printed + D (high peak force) washed conditions have potential application as energy absorbing octet-truss lattice structures.

1. Introduction

3D printing is a rapidly growing technology that allows for the production of versatile parts with geometries that can only be achieved through the additive manufacturing process. There are several stages involved in the 3D printing process, all playing a large role in developing the appropriate mechanical properties based on the targeted application of the printed part. One of the most commonly used polymers in 3D printing belong to the general family of Polymethyl Methacrylates (PMMA); in this study we have focused on the assessment of one specific type of PMMA based 3D printing polymer. PMMA blends that have been optimized for 3D printing offer an excellent balance of strength, elongation and toughness, making them suitable for functional prototypes and medical applications [1–5]. PMMA is also compatible with the stereolithography (SLA) 3D printing technique, where a structure is printed a single layer at a time through a photochemical process in which a focused UV light causes liquid chemical monomers to link together via activation and form solid polymers that make up the body of the 3D solid [2]. Once printing is completed, the part is removed from the resin bath and washed in order to remove excess resin for a more

solid and smoother product. The wash stage is then followed by a post curing treatment, in which heating or photo curing is used to achieve the desired mechanical properties of the polymer [2]. Although it is widely known that post curing increases the strength of PMMA, the effect of this treatment on elongation and toughness properties is not well documented in the literature [3]. Due to the high printing resolution and design flexibility that SLA offers and the good mechanical properties of printed PMMA parts, there is a growing field of research where this printing technique is being implemented to create repeated unit cell energy absorbing structures for use in helmet [4,6] and body protective gear [7]. On a fundamental level, a repeated array of unit cells can be optimized to produce efficient and lightweight energy absorbing structures [8], which is being exploited for application in human protective gear. Ling et al. [4] and Mohsenizadeh et al. [6] both used SLA to print PMMA octet-truss lattice structures which showed similar and better compressive energy absorption properties when compared to expanded structural foams, which these lattice structures are meant to replace in wearable protective devices. In both studies, only two different materials were considered and it was demonstrated that energy absorption was affected by (i) the arrangement/configuration of the octet-truss

* Corresponding author.

E-mail address: abardelc@uoguelph.ca (A. Bardelcik).

lattice structure and (ii) the base material mechanical properties. Due to the strong effect that base material mechanical properties have on the performance of these energy absorbing structures, identifying an appropriate post printing treatment to modify and potentially tune the PMMA mechanical properties was the motivation for the current work, where the effect of various wash treatment constituents on the tensile behavior of SLA printed PMMA material was studied. As a complement to the experimental study, the stress-strain curves extracted from the tensile tests were used to define the material properties within finite element (FE) simulations of octet-truss lattice structures, in which compression tests were modelled and analyzed to assess their energy absorption potential with respect to wash treatment.

In the proceeding literature review on the effects that wash treatments have on the mechanical properties of 3D printed polymers, it is evident that there exists a deficit in this field of research. There have been many studies based on 3D printed parts, where several different washing methods were utilized. These different wash procedures can be generalized into 5 different wash treatment categories (i) ethanol (ii) DI Water (iii) Phosphate buffered saline (PBS) (iv) Plasma treatment and (v) others (dichloromethane, acetone, hydrogel). Because of its ability to effectively remove excess resin during post-processing, ethanol wash treatments are the most commonly used [9]. Ethanol has also been used in combination with UV curing to achieve low surface roughness and high sterilization levels as shown in [10]. In another study, the adverse effects of toxicity in materials were reduced significantly after treatment with ethanol [11]. The most common ethanol wash solutions are composed of 70 % or more ethanol with the remainder consisting of DI water [12]. In 3D printing of CuSO₄ salt and poly(lactide-co-glycolide) (PLGA) to create porous structures after salt leaching, a first wash in ethanol (followed by water), resulted in dimensional growth of the printed structure, where the reverse order of the wash treatment resulted in shrinkage of the structure, which was independent of mass loss [13]. Swelling of 3D printed hydrogels was shown to be significantly greater using water rather than ethanol and it was shown that an optimized wash treatment is necessary to create defect free and mechanically strong parts [14]. Although no effects on mechanical properties are given, phosphate buffered solution (PBS) washes are typically used in biological 3D printing applications of scaffolds and stents where the removal of residual ethanol is important for compatibility with live organisms (in vivo) [15,16]. Plasma treatment is another unique wash-like method that has been applied to improve bonding of 3D printed polydimethylsiloxane (PDMS) microfluidic devices [17,18] and in surface cleaning treatments for 3D printed medical implants [19]. No indication on the effect of these plasma treatments on mechanical properties was reported. Dichloromethane (DCM) is a toxic and highly volatile compound used in solvent-cast 3D printing techniques for polylactic acid (PLA), where it was shown to toughen the material when compared to conventional fused deposition model printing of PLA [20]. Solvent evaporation affects the final printed thread diameter which has to be taken into account when considering mechanical properties. Polysulfone (PSU) and polysulfone/polyaniline (PANI) were also solvent-cast printed to show that less conventional polymers can be 3D printed using this printing method, but no mechanical properties were reported with respect to DCM concentration [21]. A multi-stage, treatment/wash of 3D printed PLA scaffolds was conducted in [22] using a variety of solutions which included ethylenediamine/n-propanol, glutaraldehyde, acetylated collagen, poly-L-lysine and DI water. This treatment procedure was shown to improve biocompatibility without sacrificing the necessary mechanical properties for the scaffold structure.

While there have been many studies which investigate the SLA 3D printing process and resulting material properties, there is a deficit in the literature on the effect of the wash stage on PMMA based material performance. Therefore, this paper will explore the toughening (or energy absorption potential) effects that different chemicals have during the washing stage of a SLA printed PMMA based material which has

been shown to have potential application as a suitable material for wearable energy absorbing lattice structures [4,6]. After a detailed discussion of the experimental and numerical methods implemented in this work, the uniaxial tensile properties of thirteen different printed and washed (various concentrations of isopropyl alcohol, hydrogen peroxide and a detergent) PMMA material conditions are quantified to assess the effect of wash treatment on the resulting mechanical properties. Detailed FE models of an octet-truss lattice structure compression test were then developed to predict the structures' energy absorption potential with respect to wash treatment.

2. Experimental and numerical methods

In this section, the 3D printing procedure, wash treatments and uniaxial tensile testing experiments are discussed.

2.1. 3D printing procedure

A Formlabs Form 2 printer was used to print miniature dog-bone tensile specimens. The Formlabs Tough resin was used in this work, which is a proprietary liquid monomeric mixture with plasticizers and upon stereolithographic photocatalysis (chain radical reactions) produces a common polymethyl methacrylate (PMMA) type hard thermoplastic with a good balance of strength and ductility. The orientation of the printed tensile specimens was 45° to the printer base as shown in Fig. 1a. Scaffolding was used to support the specimen during printing. The motivation to print the specimens at this orientation is to replicate the printing/loading orientation of the octet-truss ligaments that appear in the finite element (FE) models in this work. Also, the SLA printing technique is said to produce isotropic material properties as there is no molecular difference in terms of chemical bonds between printed layers (with respect to any print orientation) due to the absence of voids and microcracks between layers [23].

2.2. Wash treatments

A number of different wash treatment solutions were used to assess their potential effect on mechanical properties of the 3D printed material. It should be noted that no post-curing was applied to the specimens after the wash treatments. An automated Formlabs Form Wash system was used to conduct the wash treatments at ambient temperature and a wash time of 10 min. The wash was conducted immediately after the printing process. In order to assess the effect of multiple wash constituents on the subsequent mechanical properties of the specimens, a single wash solution was created and consisted of up to three different components. The three different categories of wash solutions considered in this work were:

- 1 Isopropyl Alcohol (IP) [or isopropanol]
- 2 Hydrogen Peroxide (HP)
- 3 Detergent (D) solution consisting of 0.3 wt% Sodium Caprylyl Sulfoante (Bioterge PAS-8S®), 0.2 wt% C9-C11 Alcohol Ethoxylate (Tomadol 91-6), Citric acid/KOH (pH adjusting agents), and deionized water.

Isopropyl alcohol, similar to ethanol, is another commonly used and readily available solvent for washing SLA printed objects. It provides acceptable dissolving power to cleanse unreacted liquid resin off the printed surfaces. Hydrogen peroxide is a safe and environmentally preferred oxidizing agent, which can break down to water and oxygen through reaction of its intermediate hydroxyl radical moieties. Hydrogen peroxide was included as a washing solution option considering how the polymerization reaction of PMMA occurs through photocatalytic activation of a chain radical reaction. It is likely that generation of highly reactive hydroxyl radicals by hydrogen peroxide could lead to further modification of the PMMA's surface polymer structures

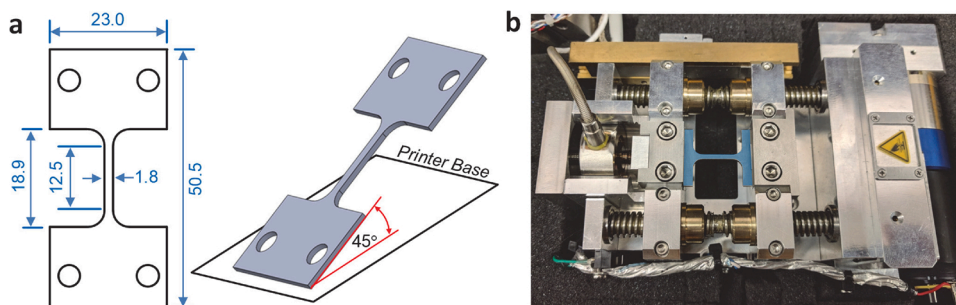


Fig. 1. (a) Miniature Dog-bone specimen geometry and print orientation (scaffolding not shown). Dimensions are in mm. (b) MTI Industries uniaxial tensile testing apparatus.

and thus its mechanical properties. Anionic and nonionic surfactants such as alkyl sulfonates and alcohol ethoxylates are also commonly sourced materials with acceptable safety and can act to modify wash solutions' effective detergency and the overall speed of a liquid's penetration/soaking as wetting agents. It is also known that most chemical reactions can be affected by the effective pH of their surroundings – the logarithmic concentration of protons in an aqueous solution. Thus, the pH of all wash solutions tested in this study were buffered to a value of 7 ± 0.1 using specific amounts of citric acid and/or KOH.

The following details pertain to a single constituent wash solution. For the Isopropanol alcohol (IP) wash, the two concentrations used in this work were 60 % and 90 % by volume as shown in Table 1, with the balance of the concentrations consisting of deionized water. The Hydrogen Peroxide (HP) wash concentrations used in this work were 2.5 % and 5 % by volume, with the balance consisting of deionized water. The Detergent (D) wash solution was used at full strength with the solution constituents detailed above.

When multiple wash constituents were considered, such as IP60 + HP5 + D as shown in Table 1, the weight percentage of the individual constituent was combined into a single solution with the balance of the wash solution consisting of deionized water. The selection of all wash solutions shown in Table 1 ensure that each variable (IP, HP, D) and at different concentrations is tested individually and in combination with one or more other variables.

2.3. Uniaxial tension testing

Uniaxial tension tests were conducted on the 3D printed dog-bone specimens. The following section briefly describes the miniature dog-

Table 1
The wash treatments considered in this work.

Condition Name	Isopropyl Alcohol (IP)		Hydrogen Peroxide (HP)		Detergent (D)
	60 %	90 %	2.5 %	5 %	
As-Printed					
Effect of IP	IP60	✓			
	IP90		✓		
Effect of HP	HP2.5		✓		
	HP5			✓	
	D				✓
Effect of Detergent	IP60 + D	✓			✓
	IP90 + D		✓		✓
	HP2.5 + D			✓	✓
Combined Effect of IP, HP and Detergent	HP5 + D			✓	✓
	IP60 + HP5	✓			✓
	IP60 + HP5 + D	✓			✓
	IP90 + HP2.5		✓	✓	✓
	IP90 + HP2.5 + D		✓	✓	✓

bone specimen geometry and equipment used to conduct the uniaxial tension tests.

2.3.1. Specimen geometry

The miniature dog-bone style specimen (Fig. 1a) used in this work was developed for aluminum sheet metal by Smerd et al. [24]. In their work, they showed that the engineering stress versus strain curves from quasi-static tension tests conducted on large scale ASTM (E8M-04) specimens with a 50 mm gauge length matched those of the miniature dog-bone specimens (12.5 mm gauge length) up to the ultimate tensile strength (UTS), where necking was observed. This was also validated by the work of Bardelcik et al. [25] for steel. Beyond the uniform elongation strain, the ratio of the neck size to gauge length results in a slightly greater total elongation for the miniature specimens, but due to the absence of a localized neck within all of the material conditions examined in this work, the authors believe it was appropriate to utilize this tensile specimen geometry. One of the major considerations for utilizing this particular specimen geometry was the reduced gauge length, width and thickness, which closely matched the ligament dimensions of the repeated cell octet-truss structure that was modelled using finite element (FE) analysis in this work.

2.3.2. Uniaxial tensile testing

An MTI Instruments SEMTester 1000 servo-electric tensile stage (see Fig. 1b) was used to conduct the tensile tests in this work. Due to the low strength of the printed material and high stiffness of the tensile stage, specimen elongation was measured using the cross-head displacement since compliance of the tensile stage is negligible in this case. By not utilizing a clip-on type extensometer, the authors realize that the test specimen elongations will include some small elastic strains which occur outside of the 12.5 mm gauge length and at the shoulders of the specimen that are contained within the 18.9 mm (Fig. 1a) gauge region. As a result, the computed engineering strains will include these small elastic strains and slightly over predict elongation when utilizing 12.5 mm as the specimen gauge length. This slightly reduces the Young's modulus of the material and as a result we measure and report the apparent Young's modulus from these test results. For all of the tests, a cross-head velocity of 0.0375 mm/s was used to deform the specimens at nominal strain rate of 0.003 s^{-1} .

For each of the material conditions shown in Table 1, five repeat tensile tests were conducted. The force and elongation data was used to compute the engineering stress-strain curves for each test. Through linear interpolation of the individual test data, a single average stress-strain curve was determined. It should be noted that the average stress-strain curves terminate at the measured average total elongation strain from the population of repeat tests. Mechanical properties such as peak stress, total elongation, toughness and apparent Young's modulus were determined for each repeat test and the average values were computed along with the standard deviation from the repeat test data. Fig. 2 shows the average and repeat test data for the As-Printed and IP90 + HP2.5 material conditions. For most of the material conditions,

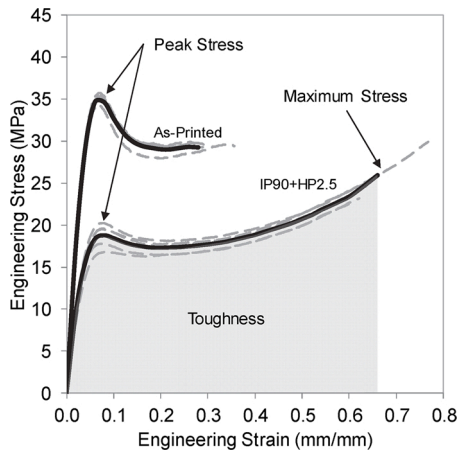


Fig. 2. The average (bold series) and individual repeat tests (dashed series) shown for the As-Printed and IP90 + HP2.5 material conditions.

the individual test repeatability was excellent as shown for the As-Printed case (Fig. 2), while the IP90 + HP2.5 case resulted in the poorest repeatability from all the material conditions tested in this work. The repeatability of each material condition is assessed by the standard deviation that is computed for each of the individual mechanical properties and will be presented in the Results section. From this point forward, only the average stress-strain curves will be presented. Peak Stress refers to the highest stress measured within the first 0.1 strain and the maximum stress refers to the highest measured stress value from the stress-strain behaviour as shown in Fig. 2. The toughness was also computed for each repeat test condition as the area under the stress-strain curve as shown Fig. 2. The effect of wash treatment on the apparent Young's modulus was also determined within the range of 5 % and 50 % of the peak stress value for each stress-strain curve. This range of stress was chosen for consistency for all of the conditions examined in this work and represented the nearly linear elastic response of the material. For the numerical portion of this work, the measured engineering stress-strain curves were converted into flow stress (true stress vs. effective plastic strain) curves and used to define the FE model material properties.

2.4. Finite element simulations

As presented in the work of Ling et al. [4], finite element (FE) simulations of compressively loaded octet-truss lattice structures were shown to accurately reproduce the experimentally measured force-displacement response of 3D printed lattice structures. A similar

FE modelling approach was conducted in this work, where the material properties (stress-strain) from the uniaxial tensile experiments were implemented within the FE models to simulate to force-displacement response of a similar lattice structure due to compressive loading. It is suitable to use the tensile data in the FE models because of the stretch dominant nature of octet-truss structures [26].

The overall geometry of the lattice structure modelled in this work is shown Fig. 3 and a close-up view of an octet-truss unit cell indicates a ligament length (L) of 9 mm and the ligament diameter (D) of 1.3 mm. In order to reduce stress concentrations and strengthen the ligament junctions, a small taper fillet was applied to the model as shown in Fig. 3. The theoretical relative density (minus taper) of this octet-truss unit cell is 0.14, as calculated using Eq. (1) from [26],

$$\bar{\rho}_{theoretical} = 6\sqrt{2}\pi \left(\frac{D}{2L}\right)^2 \quad (1)$$

The commercial dynamic-explicit FE software LS-DYNA (Ansys Incorporated) was used to conduct the compression test simulations. Although not computationally efficient, the entire lattice structure shown in Fig. 3 was modelled without the use symmetry boundary planes. Time scaling was implemented to reduce computation time and care was taken to ensure that stress wave propagation did not occur during loading. Modelling the full geometry allowed the natural and sporadic ligament buckling process to occur throughout the entire structure. A nodal displacement (negative z-direction) was applied to the ligaments located on the top plane of the structure while allowing x-y translation. The bottom plane ligaments were constrained in the z-direction only. The nodal set used to apply the vertical compression displacement was also used to extract the z-axis reaction force components that were summed to predict the compression force-displacement response for each material condition. The flow stress behaviour for each material condition was implemented utilizing the *MAT_PIECEWISE_LINEAR_PLASTICITY material card as suggested in [27]. Strain rate sensitivity was not considered in these models. Due to the complexity of the self-contact between ligaments, it was found that element erosion (via a failure criteria) resulted in a dynamically unstable condition at the point of failure, which terminated the simulations, therefore failure was not implemented in the current models. Also, even in the absence of a failure criteria, the complex ligament deformation and self-contact of the model limited the compression displacement of the lattice structures to ~8 mm (or ~22 % nominal compressive strain) prior to termination of the simulations. This level of compression was sufficient to draw meaningful conclusions on the energy absorption performance of the lattice structures that were simulated in this work and aligns with the FE model deformation level presented in [4].

A highly refined tetrahedral solid element mesh was created for this model as shown in Fig. 3. The average element size was 1.5 mm,

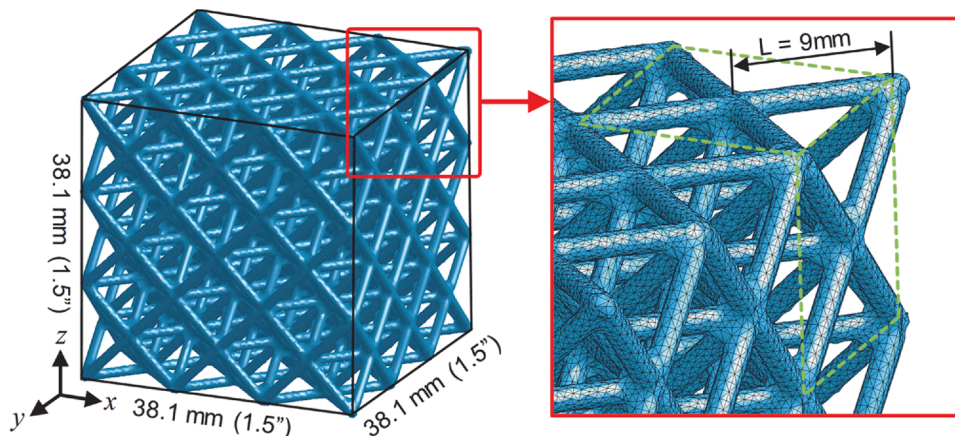


Fig. 3. The repeated cell octet-truss lattice structure used for the FE simulations.

resulting in a total of 947,208 elements used to represent the lattice structure. This highly refined element size is significantly smaller than that used in [4], therefore a convergence study was not conducted. Four-noded quadratic tetrahedron elements with nodal rotations (ELFORM 4) were implemented to model the complex ligament deformation within these models as suggested in [28]. The authors realize that these are computationally expensive simulations, and future work will consider mesh/element optimization.

3. Experimental results and discussion

The following sections present the measured stress-strain response of the 3D printed dog-bone specimens that have been subjected to the various wash treatment solutions. The effect of each individual and combined wash solution are discussed with respect to their affect on material properties. A summary of the mechanical properties observed for all of the wash solution variants is presented in Table 2 and the peak stress vs. total elongation is plotted in Fig. 4. As can be seen in Fig. 4, a large variation in mechanical properties were achieved in this work.

3.1. As-printed material properties

The as-printed stress-strain response of the PMMA material is shown in Fig. 5 and represents the baseline material condition where no wash treatment was applied. This material condition exhibits the greatest peak stress and lowest total elongation, from all of the material conditions examined in this study (Table 2). Although the peak stress is excellent (35.1 MPa), the low total elongation (0.29) resulted in the lowest (8.4 Nmm/mm³) toughness when compared to all of the material conditions examined in this work.

By simply washing the tensile specimens with the detergent solution (As-Printed + D in Table 2 and Fig. 5), the toughness increased considerably. The average peak strength was 34.5 MPa, which represented in a 2 % reduction when compared to the As-Printed material condition. A significantly higher total elongation was observed at 0.47, which represents a 62 % increase over the unwashed material condition. The increased elongation resulted in a material condition with a high toughness of 13.5 Nmm/mm³ that is 61 % greater than the unwashed material condition. The significant increase in toughness is promising when considering this material condition for 3D printed energy absorption lattice structures, especially when considering the high peak stress, which will have implications on compressive deformation response of a lattice structure as will be shown in the numerical component of this work.

It is possible that the detergent wash treatment caused partial absorption of the surfactants from the detergent solution into the polymer matrix. Considering the deterative, wetting and penetrating properties of

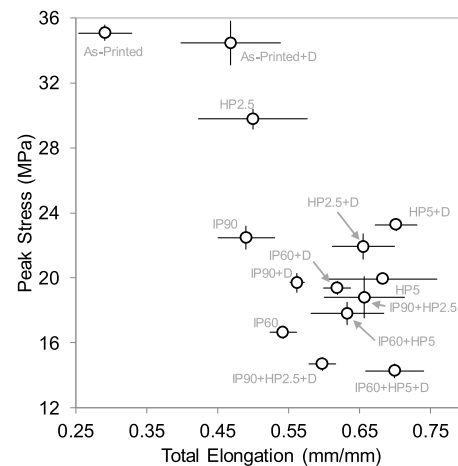


Fig. 4. The average Engineering Peak Stress vs. Average Engineering Total Elongation for all of the wash treatments examined in this work. The error bars represent the standard deviation from the population of repeat tests.

surfactant molecules, it is likely that the enhanced ductility of the polymer was due to improved intermolecular hydrocarbon gliding effects which result by interaction of the surfactant molecules with the polymeric matrices and cause plasticization. This hypothesis is supported by the work of Hargreaves [29] on notched tensile PMMA specimens that were soaked in various solutions. The results of the work showed that a surfactant (soap) solution increased the plasticization of the crack tip and resulted in the highest measured toughness index among the 12 different solutions examined in their work. On a more fundamental level, Ghebremeskel et al. [30] have also shown that surfactants can act as plasticizers in turning certain polymers (including PMMA) more plastic through solvation/plasticization.

3.2. Effect of isopropyl alcohol and detergent wash on stress-strain response

The average engineering stress-strain curves for this part of the study are presented in Fig. 5a, while the peak stress, total elongation and toughness are plotted vs. isopropyl alcohol concentration in Fig. 5b. A simple polynomial trend line is fit to the data in Fig. 5b for conversational purposes only.

3.2.1. Isopropyl alcohol effect

From this point forward, when presenting the properties of washed specimens, the values shown within the square parenthesis [] will represent the percentage increase [+] and decrease [-] compared to the

Table 2

The average mechanical properties for the various wash solution treatments. The square parentheses ([]) indicated the standard deviation from the population of repeat tests. The asterisk (*) represents that material conditions used in the finite element modelling component of this work.

	Condition Name	Average Peak Stress (MPa)	Average Total Elongation (mm/mm)	Average Toughness (Nmm/mm ³)	Average Apparent Young's Modulus (GPa)
	As-Printed *	35.1 [0.5]	0.29 [0.04]	8.4 [1.0]	0.88 [0.01]
Effect of IP	IP60 *	16.7 [0.4]	0.54 [0.02]	8.8 [0.4]	0.47 [0.02]
	IP90 *	22.5 [0.7]	0.49 [0.04]	10.1 [0.8]	0.59 [0.03]
Effect of HP	HP2.5	29.8 [0.6]	0.50 [0.08]	13.0 [2.2]	0.77 [0.04]
	HP5	19.9 [0.3]	0.68 [0.08]	13.5 [2.1]	0.54 [0.02]
	As-Printed + D *	34.5 [1.4]	0.47 [0.07]	13.5 [2.4]	0.87 [0.04]
Effect of Detergent	IP60 + D	19.4 [0.4]	0.62 [0.02]	11.9 [0.5]	0.53 [0.01]
	IP90 + D	19.7 [0.6]	0.56 [0.01]	10.5 [0.4]	0.53 [0.02]
	HP2.5 + D	21.9 [0.8]	0.66 [0.04]	13.8 [0.9]	0.53 [0.03]
	HP5 + D *	23.3 [0.4]	0.70 [0.03]	16.0 [0.7]	0.52 [0.04]
	IP60 + HP5	17.8 [0.7]	0.63 [0.05]	11.6 [1.4]	0.49 [0.03]
Combined Effect of IP, HP and Detergent	IP60 + HP5 + D *	14.3 [0.4]	0.70 [0.04]	11.4 [1.1]	0.39 [0.02]
	IP90 + HP2.5 *	18.8 [1.3]	0.66 [0.06]	12.4 [1.9]	0.46 [0.05]
	IP90 + HP2.5 + D	14.7 [0.4]	0.60 [0.02]	9.1 [0.4]	0.40 [0.02]

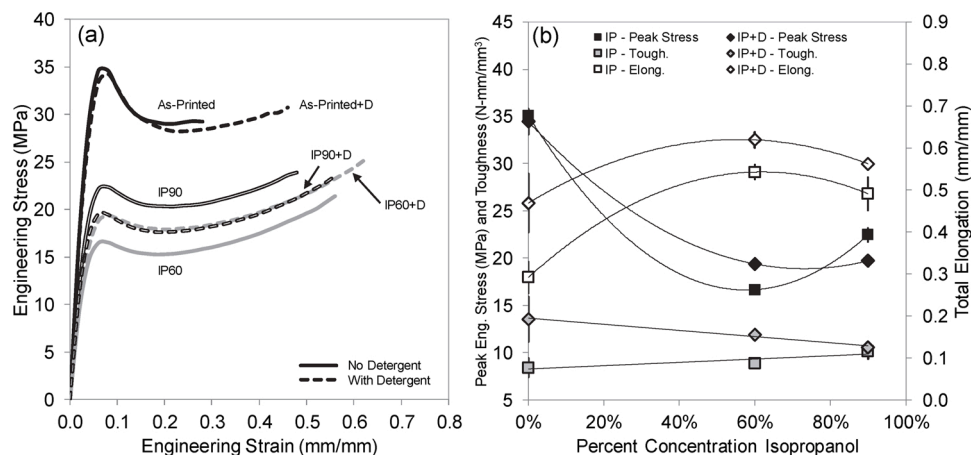


Fig. 5. Effect of Isopropyl Alcohol and Detergent wash treatment on the (a) Average stress-strain behaviour and (b) Peak Stress, Toughness and Total Elongation. The vertical error bars represent the standard deviation from the population of repeat tests.

As-Printed and unwashed material properties. The effect of a 60 % isopropyl alcohol (IP60) wash has a drastic impact on the peak stress and total elongation of the PMMA material. The peak stress reduced to 16.7 MPa [−52 %] and the total elongation increased to 0.54 [+86 %], resulting in a low toughness of 8.8 Nmm/mm³ [+5 %]. This particular wash solution resulted in the lowest toughness (after As-printed) for the entire set of wash treatments examined in this work and combined with a low peak stress, may not be a suitable material condition for use in energy absorbing lattice structure as will be shown in the numerical component of this work. It should be mentioned that this particular wash is commonly employed in 3D printing.

The observed response of the mechanical properties to the isopropyl alcohol wash are attributed to unique characteristics of polar protic organic solvents such as isopropyl alcohol which have affected the PMMA material. In the work of Andrews et al. [31], PMMA specimens were saturated (to various levels) with a number of different alcohols (methanol, ethanol, n-propanol, iso-propanol, n-butanol) and because alcohols are relatively incompatible with PMMA, they were generally found to swell rather than dissolve the polymer. Their work clearly showed that all of the alcohol treatments reduced the glass transition temperature (T_g) of the PMMA due to a plasticization effect on the polymer. The reduction in T_g also reduced the yield stress (equivalent to peak stress in the current work). Wang et al. [32] observed crack healing of PMMA due to ethanol exposure, which was also a result of T_g reduction to below the test temperature by ethanol plasticization. Vlisidis and Prombonas [33] conducted tensile tests on PMMA specimens wetted with pure alcohol and showed that a 16 % reduction in tensile strength was observed, unfortunately no insight was given with respect to the mechanisms which contributed to the strength reduction. Neves et al. [34] showed that in some polymerization reactions, the monomer-polymer conversion is incomplete, resulting in the presence of unpolymerized monomers or residual monomers (RMs). They also showed that ethanol washes with concentrations greater than 50 % resulted in a drop in the PMMA flexure strength due to the extraction of the RMs. This effect may be present within the current work where the printed (green) tensile specimens may have contained RMs. Overall, the literature suggests that alcohols have a plasticization effect on PMMA due to the reduction in T_g which aligns with the observations made in the current work, where the strength decreases and ductility increases. Without knowing the precise formulation of the proprietary Formlabs PMMA based Tough resin that was used in the current work, it is difficult to theorize on the effects that isopropanol had on the toughening plasticizers and other resin components.

By increasing the isopropyl alcohol concentration to 90 % (IP90), a strengthening effect was observed (Fig. 5a) as shown by a nearly vertical shift in the stress-strain response when compared to the IP60 material

condition. When compared to IP60, the IP90 material peak stress, total elongation and toughness changed by +35 %, −9 % and +15 %, respectively. Although IP90 exhibited better properties than IP60, the toughness of IP90 was still on the relatively low end and only +20 % better than the As-Printed material condition. At this point it is unclear why the IP90 wash resulted in a greater peak stress than the IP60 wash, but the work of Basavarajappa et al. [35] sheds some light on this phenomenon, in which a light cured glass fiber (unaffected by alcohol) composite with a complex PMMA based matrix was subject to ethanol washes at concentrations of 40 %, 70 % and 99.9 % and wash times between 15–120 s. Nano-indentation experiments were conducted to show that the surface nano-hardness and Young's Modulus (neither are bulk properties) was highest for the 70 % ethanol washed specimens, for all wash times. Although no explanation for the high properties of the 70 % ethanol wash was given, the authors suggested that the increase in surface properties was a result of reorganized polymer chains after initial swelling of the polymer surface, followed by ethanol evaporation, which may have caused crystallized regions within the PMMA matrix. Also, it was suggested that the combined solubility parameter of the ethanol-water mixtures may have altered the solubility of the PMMA surface, leading to possible crazing of the surface. The leaching of residual monomers was also suggested as a possible effect on the observed surface properties, which aligns with the findings of Neves et al. [34].

Another important aspect of the work presented by Basavarajappa et al. [35] is the effect of wash treatment time on the surface mechanical properties. They observed a strong increase in surface nano-hardness and Young's modulus as the treatment time increased from 15–120 s. This was shown for all three ethanol concentrations and it was the degree of polymer swelling (or saturation) followed by evaporation at the longer treatment times which likely resulted in the observations. This result has implications for the current research and future work will focus on the effect of wash time on the tensile properties.

3.2.2. Isopropyl alcohol + detergent effect

Although the addition of a detergent wash resulted in a total elongation increase (peak stress was unaffected) for the As-Printed material condition, the effect of adding detergent to the 60 % (IP60 + D) and 90 % (IP90 + D) isopropyl alcohol wash resulted in a peak stress increase (+16 %) and decrease (−12 %), respectively, when compared to the equivalent non-detergent isopropyl alcohol wash conditions. When compared to the non-detergent isopropyl alcohol wash conditions, the total elongation increased only slightly for both of the isopropyl alcohol + detergent conditions, therefore the IP60 + D and IP90 + D toughness was 11.9 and 10.5 Nmm/mm³, respectively. For the isopropyl alcohol and detergent washed conditions, the IP60 + D material condition represented the greatest increase in toughness when compared to

the As-Printed and unwashed condition. Although the mechanism of the IP + D effect on material properties is unknown at this time, we hypothesize that the surface active surfactant agent (D) may have enhanced the penetration of the isopropyl alcohol into the PMMA surface, resulting in this synergistic effect on toughness. Future fundamental research on this effect will be considered.

3.3. Effect of hydrogen peroxide wash concentration on stress-strain response

The average engineering stress-strain curves for this part of the study are presented in Fig. 6a, while the peak stress, total elongation and toughness are plotted vs. hydrogen peroxide concentration in Fig. 6b.

3.3.1. Hydrogen peroxide effect

The effect of a 2.5 % hydrogen peroxide (HP2.5) wash results in a small peak stress reduction to 29.8 MPa [-15 %], a noticeable total elongation increased to 0.50 [+72 %] and a relatively high toughness of 13.0 Nmm/mm³ [+55 %]. By increasing the hydrogen peroxide concentration to 5 % (HP5), a more significant drop in peak stress was observed to 19.9 MPa [-53 %], with a high increase in total elongation to 0.68 [+134 %], which resulted in a high toughness of 13.5 Nmm/mm³ [+61 %]. When compared to HP2.5, the stress-strain curve of HP5 shifts down in stress response and increases in total elongation as shown in Fig. 6a. The shape of the HP2.5 and HP5 stress-strain curves is nearly identical. This particular material conditions exhibits good mechanical properties for implementation into energy absorbing lattice structures.

In general, elongation properties of polymeric compounds could be affected by their polymer chains' type, length, and branching structure. Considering how PMMA's polymerization reaction occurs through photo activation of radical forming activators, it may be likely that further exposure of the polymer to radical generating compounds, such as hydrogen peroxide, led to post-modifications to the molecular formation of the PMMA and its surface properties [36,37]. Yavuz et al. [37] treated a PMMA microfluidic chip with hydrogen peroxide (concentration not provided) and found that both the surface roughness and glass transition temperature (T_g) of the polymer were relatively unaffected. Unfortunately, no mechanical testing was conducted and a physical interpretation if the findings was not provided. Munker et al. [38] investigated the effect of hydrogen peroxide gas plasma sterilization on the fracture properties of a 3D printed and fully cured PMMA material. They conducted 3-point bend tests and found that exposure of the PMMA to the hydrogen peroxide resulted in almost no increase of flexure strength (+2 %), but a noticeable increase in stress intensity factor (+27 %) and the total work at fracture (+34 %) which aligns with the trends observed in the current work where toughness increased for

increasing HP wash concentrations. Again, no discussion of the molecular effects of the PMMA brought upon by the exposure to hydrogen peroxide plasma was presented in this work.

3.3.2. Hydrogen peroxide + detergent effect

When compared to the HP2.5 case, the effect of adding detergent to the wash (HP2.5 + D) resulted in a material peak stress, total elongation and toughness changed by -27 %, +32 % and +6 %, respectively. Although the difference in toughness (or energy absorption capacity) is relatively small between the two cases, the higher peak stress of the HP2.5 case is more desirable from an energy absorption perspective.

The HP5 + D stress-strain behavior exhibits a +17 % increase in peak stress when compared to the HP5 case. There is almost no change in total elongation for the HP5 and HP5 + D cases, which results in a +19 % increase in toughness for the HP5 + D material condition when compared to the HP5 case. The actual toughness of the HP5 + D material condition is 16.0 Nmm/mm³ [+90 %] and represents the highest observed toughness from all of the material conditions examined in this work, resulting in desirable properties due to a combination of high toughness and moderate peak stress. The lack of literature on the interaction of HP on PMMA makes it difficult to hypothesize the effect of the HP + D on the observed mechanical properties, but as mentioned in Section 3.2.2, the active surfactant agent (D) may have enhanced the penetration of hydrogen peroxide into the PMMA surface, resulting in the synergistic boost in toughness for this combined wash treatment. This phenomenon warrants further study on a fundamental level.

3.4. The combined effect of isopropyl alcohol and hydrogen peroxide wash concentration on stress-strain response

Two different combined isopropyl alcohol and hydrogen peroxide wash treatments were selected for this study. The IP60 + HP5 case represented a wash solution consisting of the lowest IP (60 %) and highest HP (5 %) case. The second wash solution was IP90 + HP2.5 and represented the highest IP (90 %) and lowest HP (2.5 %) case. For both of these solutions, a detergent case was also considered. The average engineering stress-strain curves and the peak stress, total elongation and toughness for the combined isopropyl alcohol and hydrogen peroxide wash treatments are presented in Fig. 7.

Interestingly, the IP60 + HP5 and IP90 + HP2.5 material conditions resulted in a similar stress-strain response as shown in Fig. 7a. The peak stress, total elongation and toughness for the IP60 + HP5 material condition was 17.8 MPa [-50 %], 0.63 [+117 %] and 11.6 Nmm/mm³ [+38 %], respectively. For the IP90 + HP2.5 material condition, the peak stress, total elongation and toughness was 18.8 MPa [-46 %], 0.66 [+128 %] and 12.4 Nmm/mm³ [+48 %], respectively. The slightly

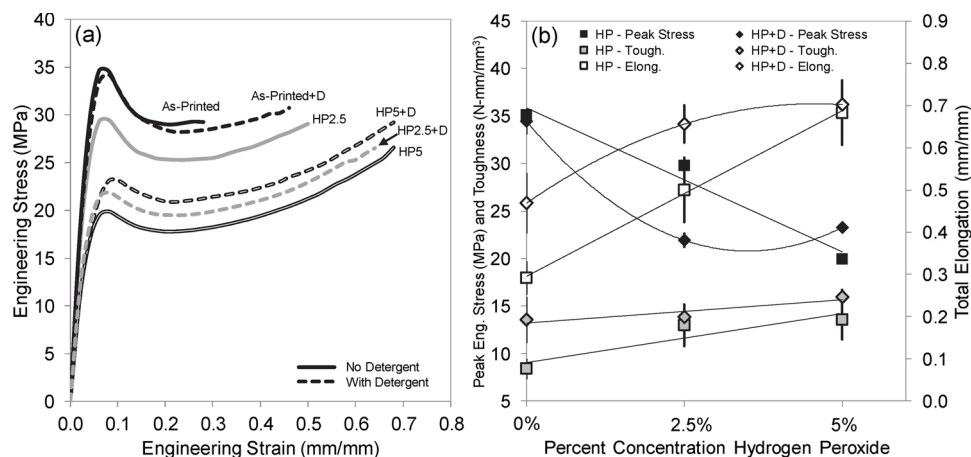


Fig. 6. Effect of Hydrogen Peroxide and Detergent wash treatment on the (a) Average stress-strain behaviour and (b) Peak Stress, Toughness and Total Elongation. The vertical error bars represent the standard deviation from the population of repeat tests.

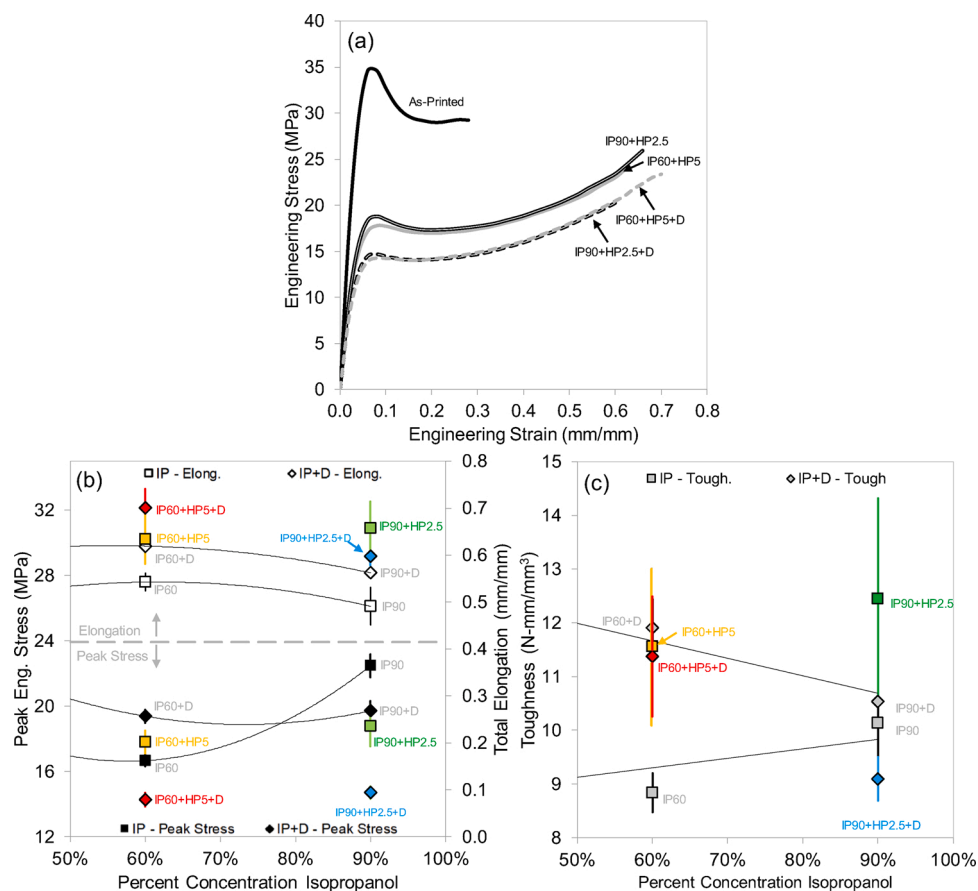


Fig. 7. Effect of the combined Isopropyl alcohol, Hydrogen Peroxide and Detergent wash treatments on the (a) Average stress-strain behaviour and (b) Peak Stress and Total Elongation and (c) Toughness. The vertical error bars represent the standard deviation from the population of repeat tests.

higher peak stress and total elongation of the IP90 + HP2.5 material condition resulted in a mild increase in toughness for this case. When compared to the isopropanol wash only, both the IP60 + HP5 and IP90 + HP2.5 cases resulted in a marginal change in peak stress, but a noticeable increase in total elongation, which resulted in the improved toughness for these two cases as shown in Fig. 7c. This result is likely due to the combined effects of the IP and HP on PMMA polymer molecules, causing structural modifications to the construct and plasticizer functions within the PMMA material. The exact molecular and intramolecular effects causing these observations remain to be determined.

The addition of detergent to the wash of these two cases also produced a very similar stress-strain response as shown in Fig. 7a. The main difference between the two cases is the total elongation, which was 0.70 [+141 %] for IP60 + HP5 + D and 0.60 [+107 %] for IP90 + HP2.5 + D case respectively. The peak stress for these two conditions were the lowest measured from the entire set of conditions examined in this work, at approximately 14.5 MPa, which is less than 50 % of the As-Printed material condition. As a result, the toughness of these material conditions was low and represents undesirable mechanical properties for implementation within energy absorbing lattice structures. The addition of detergent clearly reduced the strength of these combined IP + HP cases as shown in Fig. 7a. When compared to the isopropanol wash only, a drop in peak stress and increase in elongation for the IP60 + HP5 + D resulted in a similar toughness as IP60 + D, while the more significant reduction in peak stress for the IP90 + HP2.5 + D and only marginal increase in elongation resulted in a noticeable drop in toughness when compared to IP90 + D as shown in Fig. 7c. It is likely that these specific wash solution compositions were affected by the aforementioned mechanism of the detergent component enhancing the plasticization and penetration of PMMA, along with further not well understood

effects resulting from having IP and HP present in the same wash solution.

3.5. Relative ranking of all wash conditions

Based on the results from all of the wash treatments applied to the As-Printed PMMA material considered in this work, the relative ranking of toughness (energy absorption) and peak stress properties is presented in Fig. 8. Fig. 8a is a normalized ranking of toughness based on the As-Printed material condition which is represented by a value of 1. The bar graph clearly shows that the As-Printed material had the lowest measured toughness from the 14 different material conditions examined in this work. Although the peak stress was the highest for this material conditions, the low total elongation resulted in the lowest toughness. The simple addition of detergent to the As-Printed wash (As-Printed + D) greatly improved the toughness due to enhanced elongation of this material condition, which ranked 3rd highest as shown in Fig. 8a. In a general sense, the hydrogen peroxide washed materials (with and without detergent) all ranked near the top of the toughness rank due to the excellent improvement in total elongation with only a moderate drop in peak stress. From a toughness perspective, the HP5 + D material condition resulted in a toughness that is 90 % greater than the As-Printed material condition. Due to a moderate increase in total elongation and a moderate decrease in peak stress, the isopropyl alcohol washed materials (with and without detergent) ranked on the lower end of the toughness spectrum for the entire set of conditions examined in this work, with the IP60 + D material ranking 7th. The combined isopropyl alcohol and hydrogen peroxide wash treatments ranked approximately in the middle of the toughness ranking due to their incredibly high total elongations, but at the cost of a high peak stress

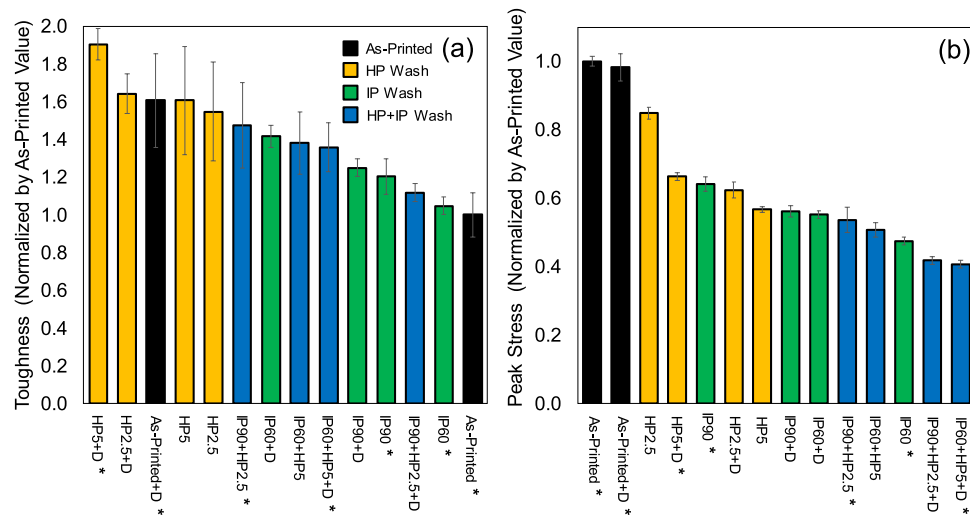


Fig. 8. Ranking of the (a) Toughness and (b) the Peak Stress for all of the material conditions considered in this work. The data in both graphs is the average data and normalized by the value of the As-Printed material condition. The error bars represent the standard deviation from the population of repeat tests.

decrease.

Although the measure of a materials' toughness (from base material tensile tests) represents the total energy absorption potential of that specific base material condition, it does not provide any insight into the potential energy absorption performance of an octet-truss lattice structure, when that material condition is used to produce the structure. The importance of understanding the effect of a materials' peak stress and toughness on its compressive energy absorption performance in a protective wear application is highlighted in the work of Di Landro et al. [39], where expanded polystyrene (EPS) foams used for protective helmets were investigated. It was shown that high-density foams (which exhibited high peak strength and moderate ductility) were able to absorb more energy than low peak strength and very ductile low-density EPS foams. However, the high-density foams exhibited a high rate of energy absorption and transferred higher accelerations and forces locally at the impact point of the helmet which leads to a critical design consideration for wearable energy absorbing applications. Therefore, a balance of good toughness and peak stress (which controls acceleration) must be considered in an energy absorbing material. Fig. 8b was constructed to rank the peak stress (normalized by As-Printed material condition) for all of the wash conditions. It is clear that the two As-Printed material conditions exhibit the highest peak stresses, but at vastly different relative toughness values as shown in Fig. 8a. In general, the HP and HP + D conditions exhibit moderate peak stress values and excellent toughness properties within this group of measured properties, which may make them a desirable candidate material condition for application within an energy absorbing octet-truss structure. With the exception of IP90, the remaining IP and combined IP + HP material conditions rank in the lower half of the chart. These rankings of base material toughness and peak stress from tensile tests will be revisited in the discussion of the octet-truss compression model results, where the predicted energy absorption performance (total energy absorbed and rate of energy absorption, or transmitted acceleration) will be compared to the tensile data.

4. FE simulation results

The compression test FE simulations conducted on the octet-truss lattice structures are presented in this section of the work for seven of the material conditions, which span the range in toughness measured from the tensile tests. These material conditions are indicated by the asterisk (*) in Table 2 and Fig. 8.

4.1. FE simulation results

The compression force-displacement data extracted from the models is presented in Fig. 9 as the individual data points (central 3-point average applied). Utilizing non-linear regression analysis, a 4th order polynomial was fit to the raw numerical data up to 7 mm of displacement as shown by the solid curves in Fig. 9. The FE models were able to predict the initial rise in force with relatively low scatter up to the peak force for all of the models. The peak force represents the displacement just prior to the start of ligament buckling/collapse within the lattice structure, which increased the scatter of the force data due to significant bending/self contact of the ligaments and dynamic effects. By dividing the peak force by the cross sectional area of the lattice structure (1,452 mm² or 2.25 in²), the equivalent of a yield stress for the lattice structures can be calculated since ligament collapse would have occurred just after this displacement. At a displacement of 6.5 mm, the structure had been deformed by a distance of one full row of the repeat unit cells as shown in Fig. 10a. This level of displacement represents the approximate minimum in the force response, which begins to increase with further displacement due to the engagement of a second row of unbuckled lattice cells. As shown by the lattice structure images in Fig. 10a at a displacement of 6.5 mm, the As-Printed (and As-Printed + D) lattice structures failed through the collapse of approximately one row of unit cells, while the lower peak force lattice structure IP60 + HP5 + D initiated collapse through multiple rows, which was also observed for all of the other material conditions modelled. Fig. 10b compiles the average force-displacement curves and a distinct peak force is shown for all of the material conditions. The As-Printed and As-Printed + D material conditions result in the highest peak force, while the IP60 + HP5 + D lattice structure represents a significantly lower peak force. The relationship between the peak force observed in the FE simulations and the peak stress from the tensile testing experiments for these material conditions is shown in Fig. 11a. Based on these results, it is obvious that a strong linear relationship exists between the peak force and peak stress as show by the linear regression (dashed line) that was fit to the data.

Energy absorption (or energy-displacement curve) during the compression simulation can be expressed by integrating the average force-displacement curve as shown in Figs. 9 and 10c. Clearly, the As-Printed and As-Printed + D lattice compression energy-displacement response is the greatest due to the high peak force. When considering a displacement of 6.5 mm (or when the force-displacement is approximately minimum), the total amount of energy absorbed by the As-

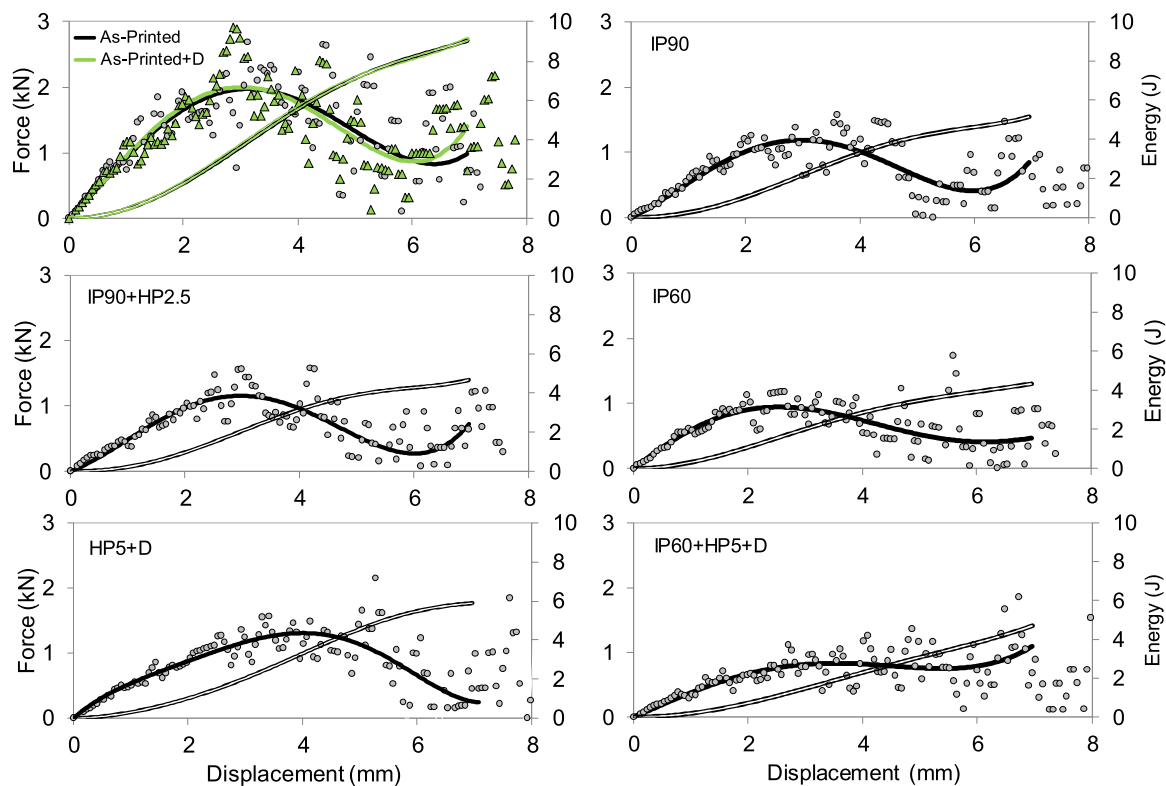


Fig. 9. The predicted force-displacement data for the 6 material conditions considered in this work. The solid black curve represents the average force-displacement response of the models and the double line curve represents the average energy-displacement response.

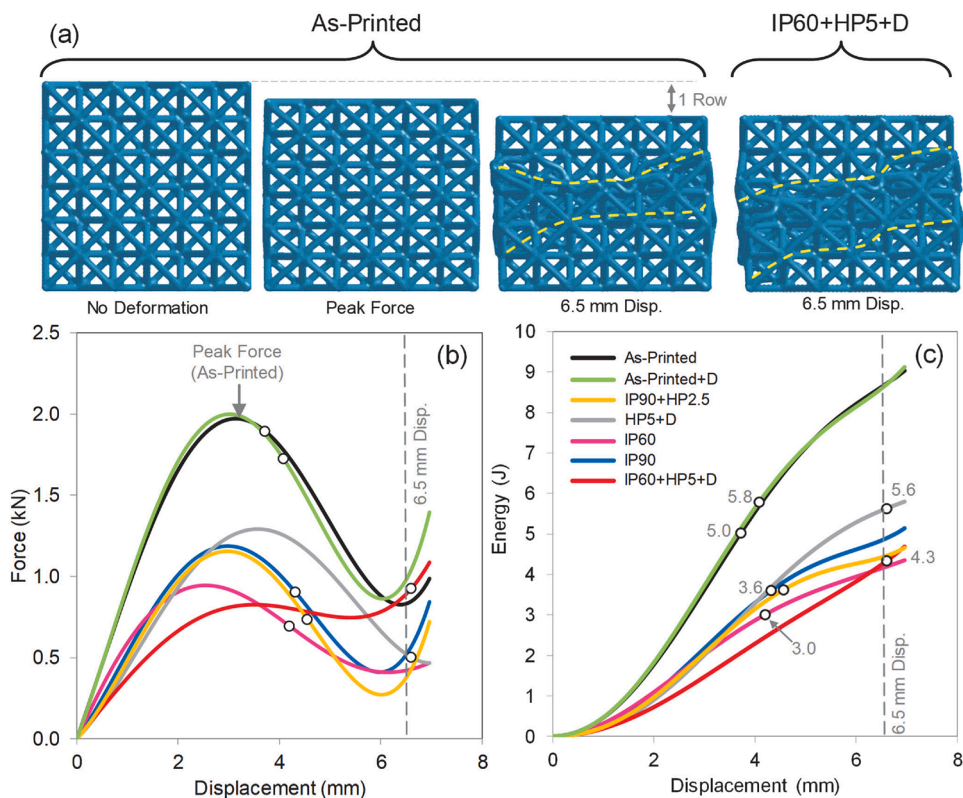


Fig. 10. (a) Images of the deformed lattice structures and a comparison of the (b) average force-displacement and (c) energy-displacement curves for the material conditions examined in the numerical work. The open data points indicated the displacement where the predicted strain exceeded the total elongation strain of the material from the tensile tests.

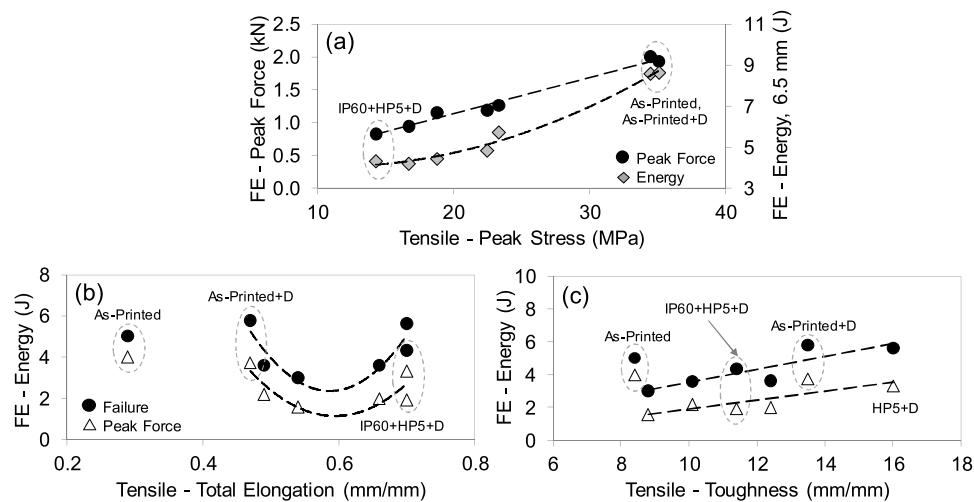


Fig. 11. Tensile test and FE simulation relationships for (a) FE-Peak Force vs. Tensile-Peak Stress (b) FE-Energy vs. Tensile-Total Elongation (c) FE-Displacement vs. Tensile Total Elongation (d) FE-Energy vs. Tensile Toughness.

Printed lattice structure is more than double that of the lowest peak stress (from tensile test) IP60 + HP5 + D material condition. Due to the nearly sinusoidal force-displacement response and the relative peak force reduction at 6.5 mm displacement for each material condition (Fig. 10b), a second order polynomial relationship with respect to the tensile test peak stress exists as shown in Fig. 11a. As a reminder to the reader, failure (element erosion) is not included in these models, therefore the energy absorbed at 6.5 mm of displacement is likely less than that reported in this work for some of the material conditions.

Keeping the previous consideration in mind, the total elongation strain (converted to effective plastic strain) from the tensile tests was used to determine (through inspection) the displacement at which the first ligament within the lattice structure would have failed. Only tensile failure strains were considered, while compressive strains were assumed to delay catastrophic fracture and were neglected in this simple failure analysis. The authors acknowledge that this is a simplified method of determining ligament failure, but acts as a relative comparison for the models examine in this work. For the As-Printed material only, the low tensile total elongation (see Table 2) resulted in tensile loading failure of a ligament as shown in Fig. 12. All of the other material conditions presented ligament failure due to a combined tensile-bending stress-state at the connection point of the ligaments (node), which are pulled in tension and have also experienced rotation of the node due to buckling of neighboring ligaments as shown for IP90 in Fig. 12. These two failure modes were observed for compressed octet-truss lattice structures as presented in [4,6]. Of course, severe bending did occur within the majority of buckled ligaments as shown for IP60 + HP5 + D in Fig. 12, but the high ductility of this material condition resulted in high compressive bending strains (failure not considered) and moderate tensile bending

strain that did not exceed our simple failure strain criteria. The lattice displacement at which a ligament would have failed is shown by the open data points in Fig. 10b and c for the force-displacement and energy-displacement curves. The highest failure displacement occurred for the IP60 + HP5 + D and HP5 + D material conditions, which is expected due to the high total elongation (0.70) of these material conditions as shown in Table 2. We believe that these two materials would likely not fail in a real component, resulting in an intact recovery of the lattice structure.

In an attempt to relate the predicted energy absorption of the lattice structures to the tensile properties of the material conditions modelled, a plot of the lattice energy absorbed at the (1) peak force displacement and (2) failure displacement is shown with respect to the total elongation of each material condition as measured from the tensile tests is shown in Fig. 11b. With exception of the As-Printed material condition, the remainder of the material conditions resulted in a polynomial fit of the data for both the lattice structure peak force and failure displacements. The correlations suggest that within the bounds of the tensile properties of the material conditions tested in this work, a minimum lattice energy absorption would occur for the material conditions with total elongations around 0.60. A more intuitive relationship is shown in Fig. 11c, where the predicted lattice energy absorption at the peak force and failure condition is plotted with respect to the tensile test toughness measured for each material condition. Again, the As-Printed material condition results were excluded from the regression analysis, which showed that a linear relationship exists between tensile toughness and FE energy absorption at peak force, but a non-linear correlation was found between the tensile toughness and FE energy absorption at failure. Considering this energy-toughness relationship, the As-Printed lattice

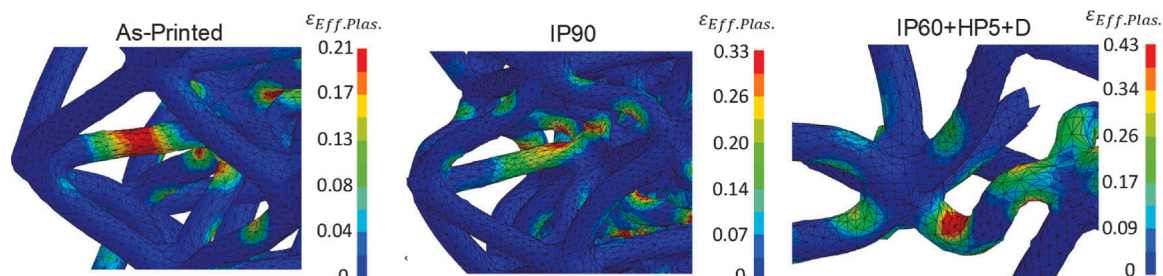


Fig. 12. Effective plastic strain contours showing the first failed ligament in the As-Printed and IP90 lattice model. A severely buckled ligament in the IP60 + HP5 + D model (surrounding elements removed for clarity). All of the maximum strain contours are set to the average elongation strain (converted to effective plastic strain) extracted from the tensile tests for those material conditions.

structure appears to possess an excellent energy absorption potential, which was not captured by the low toughness of this material condition as shown in Fig. 8a. A high toughness material condition may possess excellent energy absorption potential as shown by HP5 + D in Fig. 12c, but the effect of the relatively moderate peak force (or yielding stress of the lattice structure) has yet to be discussed with respect to the rate of energy absorption (or transmitted acceleration, see Section 3.5) when compared to the As-Printed lattice structure which has comparable energy absorption, but a higher peak force.

Considering the base material tensile test toughness and peak stress ranking presented in Fig. 8, the As-Printed + D and As-Printed material conditions resulted in the highest tensile peak stress and in Fig. 10c, they also predicted a high lattice energy absorption of 5.8 and 5.0 J, respectively. Although these two materials resulted in failure at the lowest compression displacement (Fig. 10b), it was the high energy absorption rate of these materials which allowed them to absorb a high level of energy. Even though this is a good result in terms of total energy absorbed, the high rate of energy absorption will induce the highest (relative to the materials examined in this work) accelerations transmitted through the energy absorber, which may be undesirable. The remaining material conditions exhibit a similar and lower energy absorption rate until the point of failure but at the cost of lower levels of absorbed energy. The exception to this is the HP5 + D lattice structure which absorbed a very high 5.6 J of energy at the lower energy absorption rate due to the base material exhibiting a high toughness (Fig. 8a) and moderate peak stress (Fig. 8b). The IP60 + HP5 + D lattice predicts the lowest energy absorption rate and a high total energy absorbed, but this is likely a misleading result due to the high scatter of the FE force-displacement data and non-sinusoidal average fit to the data as shown in Fig. 9. Relatively speaking, the octet-truss FE models show that the ranking of energy absorption rates (or transmitted accelerations) align with the base material tensile peak stress rankings that were presented in Fig. 8b, while a base materials' tensile toughness ranking does not consistently align with the predicted energy absorbed at the point of failure, as highlighted by the two As-Printed cases in Fig. 11c.

4.2. Comparison of FE models to published octet-truss compression test experiments

In this part of the work, we compare our FE model results to published experimental compression test (similar 3D printed octet-truss structure) data in an effort to demonstrate that the FE modelling approach we have taken is suitable to assess the energy absorption potential of such structures when exposed to different wash treatments. Also, we assess the compression test performance of the Formlabs Tough PMMA resin (and wash treatment) used in this work against two other

SLA 3D printed resin materials and an EPS foam for reference.

In the work of Ling et al. [4,40], the energy absorption of 3D printed (SLA) octet-truss structures was measured and compared to Expanded Polystyrene (EPS) foam, which is a widely used energy absorbing material and has been implemented in head protective helmets [39]. The printed and tested lattice structures in [4] had a ligament length (L) of 10 mm and ligament diameter of 0.14 mm (for R = 0.7 mm case), resulting in a $\bar{\rho}_{theoretical} = 0.13$. This is a very similar lattice structure to the one simulated in this work, where $\bar{\rho}_{theoretical} = 0.14$. The compression surface area was ~125 % greater than the area of the simulated structure in this work and the height was also ~50 % greater than in the FE models. To normalize the energy absorption response of these lattice structures, the nominal compressive stress-strain was calculated from the FE models and compared to the measured compression stress-strain response (digitized data) for the lattice structure from [4] and presented in Fig. 13a. The stress-strain response of the printed and tested lattice structures from [4] showed a very similar response to the material modelled in this work. The "Standard" resin lattice structure exhibited low engineering strain at failure, which was a result of the high tensile strength and brittle (true total elongation from tensile test was ~0.10) base material tensile properties resulting from the printing and curing of this resins. The failure modes were not detailed in [4], but it is likely that tensile ligament failure occurred prior to reaching a peak stress, therefore the predicted As-Printed + D stress-strain response is more desirable due to the enhanced ductility which would have resulted in a higher lattice strain at failure based on the FE models and likely absorbed more energy. The "Durable" resin material properties have a very similar base material tensile stress-strain response to IP60 + HP5 + D, hence the similarity of the lattice structure stress-strain curves shown in Fig. 13a. The lower peak stress of the predicted IP60 + HP5 + D lattice structure could be a result of geometric effects introduced by the considerable smaller FE modelled lattice structure.

The Specific Energy Absorption (SEA) of a material is quantified by dividing the absorbed energy ($E_{Absorbed}$) during compression by the mass ($m_{Structure}$) of the tested structure as shown here,

$$SEA = \frac{E_{Absorbed}}{m_{Structure}} \quad (2)$$

This metric is used to assess the energy absorption capacity of materials/structures where lightweighting applications are sought, which is the case for these structures that have potential applications in protective wear. Using a printed density of 1.18 g/cm³ (as per Formlabs) for the resin used to print the tensile specimens in this work, the predicted SEA of three lattice structures are shown in Fig. 13b, along with the measured SEA for the printed and tested lattice structures from [4] (digitized data). Also digitized from [4] is the SEA for two different density EPS foams that are discussed in [40]. As expected, the SEA of the

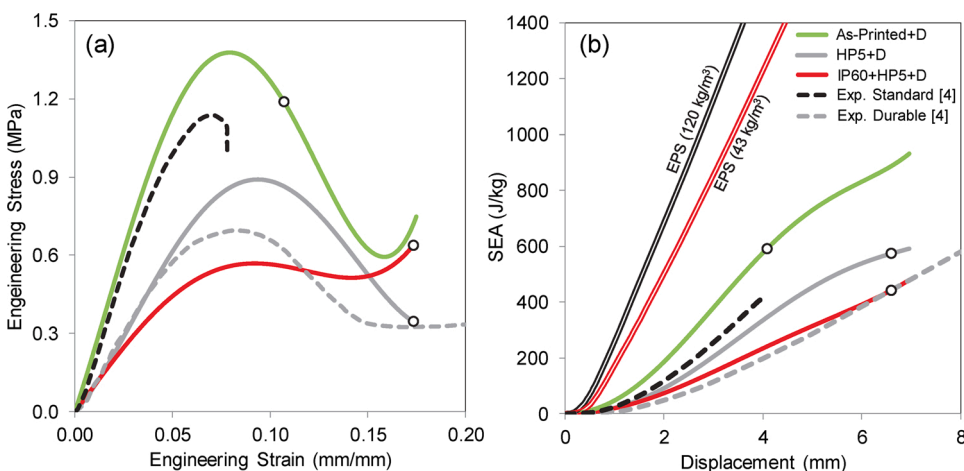


Fig. 13. (a) A comparison of the predicted stress-strain response and the measured stress-strain for an experimentally printed and tested lattice structure (R = 0.7 mm) made from a "Standard" resin (Sample 1) and "Durable" resin (Sample 3) as presented in [4]. (b) The predicted Specific Energy Absorption (SEA) and the measured SEA for an experimentally printed and tested lattice structure (R = 0.7 mm) made from a "Standard" resin and "Durable" resin as presented in [4]. The SEA of EPS foam is also presented from [4]. All of the data shown here from [4] was digitized. The open data points indicate the displacement where the predicted strain exceeded the total elongation strain of the material from the tensile tests.

tested Durable lattice structure and the predicted IP60 + HP5 + D lattice structure SEA is similar due to similarity in the tensile stress-strain response. The open data points represent the displacement at which failure may occur for the predicted lattice structures and indicates that the As-Printed + D structure may fracture at a similar displacement to the Standard resin structure, but at an elevated energy absorption per unit mass, resulting in a more desirable performance. The SEA of the EPS foams is greater than all of the printed and predicted lattice structures due to the extremely light weight of this cellular material, but is unable to recover from compressive deformation due to the fracture of the cellular structure, hence remaining near the deformed shape. Based on the material properties of the printed lattice structures, it has been shown that geometric recovery of the compressed octet-truss structures occurs and is beneficial for repeated impact loading conditions, such as those experienced in protective wear [4,6]. The Durable SEA (Fig. 13b) was shown to partially recover, therefore the FE models indicate that more promising energy absorption performance may be obtained by a lattice structure that has been washed in HP5 + D. It is the higher peak stress and excellent elongation of the HP5 + D material condition which allows for greater energy absorption and possible structural recovery. Based on the FE simulations conducted in this work, the promising potential to tune the lattice energy absorption and SEA with respect to a simple wash condition has been shown and will be validated through future experimental work.

5. Conclusions

Based on the experimental and numerical results presented in this article, the following conclusions can be made:

- 1 The effect of a simple detergent wash (As-Printed + D) resulted in a 61 % increase in toughness when compared to the As-Printed and unwashed material condition. This enhancement is due to an increase in total elongation only (peak stress remained relatively unchanged), which is a possible result from the interaction of the surfactant molecules to plasticize the PMMA.
- 2 A 60 % isopropyl alcohol (IP60) wash resulted in a degradation (−50 %) in peak stress, an increase (+82 %) in total elongation and relatively no change in toughness when compared to the As-Printed material properties. These properties resulted in a material with no positive benefit with respect to energy absorption. A 15 % increase in toughness (compared to IP60) was observed for the 90 % isopropyl alcohol (IP90) wash, which was a result of increased strength and only a slight improvement in total elongation. It is likely that exposure of the PMMA to the isopropanol caused a plasticizing effect by reducing the glass transition temperature (T_g) of the polymer. The addition of detergent resulted in an improvement in toughness for IP60 + D and nearly no toughness change for IP90 + D.
- 3 The hydrogen peroxide washes resulted in a more positive effect on the toughness of the material response when compared to the properties due to the isopropyl alcohol wash treatments. For all of the HP and HP + D wash treatments, a reduction in strength and a considerable increase in total elongation (when compared to As-Printed) was observed, which resulted in excellent toughness properties. Although the precise molecular modification of the PMMA due to HP exposure is unknown at this time, it has been established that a radical generating compound such as hydrogen peroxide leads to the modification of the PMMA polymer molecules, as demonstrated by the observed mechanical properties. The toughness of the HP5 + D material condition was 16.0 Nmm/mm³ (+90 % greater than As-Printed) and represented the highest observed toughness from all the material conditions examined in this work, resulting in desirable energy absorption properties.
- 4 The combined wash treatments consisting of isopropyl alcohol and hydrogen peroxide, resulted in significant reductions in peak stress, but an improvement in total elongation when compared to the As-

Printed material condition. This combination of properties resulted in a mild increase in toughness. The addition of detergent to the combined wash treatments resulted in a drop in peak stress, with little to no increase in total elongation, resulting in no significant benefit in terms of toughness. These observations were due to the complex and synergistic effects that the combined solutions had on the PMMA polymer molecules.

- 5 Finite element simulations of compression tests were conducted on repeated octet-truss lattice structures (using measured stress-strain properties) and showed that a linear relationship exists between the predicted lattice structure peak force and the peak stress measured from the tensile tests. Also, the predicted energy absorption potential of the lattice structures was shown to be linearly related to the toughness measured from the tensile tests, confirming that a wash treatment with excellent toughness (such as HP5 + D and As-Printed + D) would be a suitable candidate for energy absorption applications. From a design perspective, the energy absorption rate defines the transmitted accelerations, therefore the moderate energy absorption rate and high total energy absorbed of the HP5 + D lattice make this an ideal candidate (within the materials examined in this work) for potential application as a wearable energy absorber. Future experimental work will be conducted to validate these models and findings.

CRedit authorship contribution statement

Alexander Bardelcik: Conceptualization, Formal analysis, Data curation, Writing - original draft, Writing - review & editing. **Steven Yang:** Investigation, Data curation. **Faraz Alderson:** Conceptualization, Methodology, Resources, Writing - original draft, Writing - review & editing. **Andrew Gadsden:** Conceptualization, Resources, Writing - review & editing, Supervision, Funding acquisition.

Declaration of Competing Interest

Faraz Alderson is employed by Virox Technologies Incorporated. Virox donated the chemicals used in this research. No funding was provided by Virox for this research.

Acknowledgements

Funding for this project was provided by the Natural Sciences and Engineering Research Council of Canada (NSERC). The authors would like to acknowledge Virox Technologies for their generous donation of the wash chemicals used in this study.

References

- [1] C. Polzin, S. Spath, H. Seitz, Characterization and evaluation of a PMMA-based 3D printing process, *Rapid Prototyp. J.* 19 (1) (2013) 37–43.
- [2] J.-Y. Lee, J. An, C.H. Chua, Fundamentals and applications of 3D printing for novel materials, *Appl. Mater. Today* 7 (2017) 120–133.
- [3] Z. Zguris, How Mechanical Properties of Stereolithography 3D Prints Are Affected by UV Curing, Formlabs, 2017 [Online], Available: <https://formlabs.com/media/upload/How-Mechanical-Properties-of-SLA-3D-Prints-Are-Affected-by-UV-Curing.pdf> [Accessed 22 September 2019].
- [4] C. Ling, A. Cernicchi, M.D. Gilchrist, P. Cardiff, Mechanical behaviour of additively-manufactured polymeric octet-truss lattice structures under quasi-static and dynamic compressive loading, *Mater. Des.* 162 (2019) 106–118.
- [5] G.L. Chakkalakal, M. Alexandre, A. Boschetti-de-Fierro, V. Abetz, Effect of silica-coated poly(butyl methacrylate)-block-poly(methyl methacrylate) double-shell particles on the mechanical properties of PMMA composites, *Macromol. Mater. Eng.* 297 (2012) 887–893.
- [6] M. Mohsenizadeh, F. Gasbarri, M. Munther, A. Beheshti, K. Davami, Additively-manufactured lightweight metamaterials for energy absorption, *Mater. Des.* 139 (2018) 521–530.
- [7] J. Brennan-Craddock, D. Brackett, R. Wildman, R. Hague, The design of impact absorbing structures for additive manufacture, *J. Phys. Conf. Ser.* 382 (2012).
- [8] M.C. Messner, Optimal lattice-structures materials, *J. Mech. Phys. Solids* 96 (2016) 162–183.

- [9] Y. He, W.-B. Wu, J.-Z. Fu, Rapid fabrication of paper-based microfluidic analytical devices with desktop stereolithography 3D printer, *RSC Adv.* 5 (4) (2015) 2694–2701.
- [10] H.N. Chan, Y. Chen, Y. Shu, Y. Chen, Q. Tian, H. Wu, Direct, one-step molding of 3D-printed structures for convenient fabrication of truly 3D PDMS microfluidic chips, *Microfluid. Nanofluidics* 19 (1) (2015) 9–18.
- [11] F. Alifui-Segbaya, S. Varma, G.J. Lieschke, R. George, Biocompatibility of photopolymers in 3D printing, *3D Print. Addit. Manuf.* 4 (4) (2017) 185–191.
- [12] F.M. Michel, J.D. Rimstidt, K. Kletetschka, 3D printed mixed flow reactor for geochemical rate measurements, *Appl. Geochem.* 89 (2018) 86–91.
- [13] A. Jakus, N. Geisendorfer, P. Lewis, R. Shah, 3D-printing porosity: a new approach to creating elevated porosity materials and structures, *Acta Biomater.* 72 (2018) 94–109.
- [14] A. Hiller, K. Borchers, G.E. Tovar, A. Southan, Impact of intermediate UV curing and yield stress of 3D printed poly(ethylene glycol) diacrylate hydrogels on interlayer connectivity and maximum build height, *Addit. Manuf.* 18 (2017) 136–144.
- [15] D. Liu, W. Nie, D. Li, W. Wang, L. Zheng, J. Zhang, J. Zhang, C. Peng, X. Mo, C. He, 3D printed PCL/SrHA scaffold for enhanced bone regeneration, *Chem. Eng. J.* 362 (2019) 269–279.
- [16] A.J. Guerra, P. Cano, M. Rabionet, T. Puig, J. Ciurana, Effects of different sterilization processes on the properties of a novel 3D-printed polycaprolactone stent, *Polym. Adv. Technol.* 29 (8) (2018) 2327–2335.
- [17] A.K. Au, N. Bhattacharjee, L.F. Horowitz, T.C. Chang, A. Folch, 3D-printed microfluidic automation, *Lab Chip* 15 (8) (2015) 1934–1941, <https://doi.org/10.1039/c5lc00126a>.
- [18] H.N. Chan, Y. Chen, Y. Shu, Y. Chen, Q. Tian, H. Wu, Direct, one-step molding of 3D-printed structures for convenient fabrication of truly 3D PDMS microfluidic chips, *Microfluid. Nanofluidics* 19 (1) (2015) 9–18.
- [19] L. Guo, Z. Xie, H. Yao, Y. Wang, A comparative study of surface cleaning treatments for 3D printed medical implants, Volume 1: Development and Characterization of Multifunctional Materials; Mechanics and Behavior of Active Materials; Bioinspired Smart Materials and Systems; Energy Harvesting; Emerging Technologies (2017). R. Passieux, L. Guthrie, S.H. Rad, M. Lévesque, D. Therriault, F.P. Gosselin, Microstructured fibers: instability-assisted direct writing of microstructured fibers featuring sacrificial bonds, *Adv. Mater.* 27 (24) (2015) (Adv. Mater. 24/2015) pp. 3708–3708.
- [21] Z. Miao, J. Seo, M.A. Hickner, Solvent-cast 3D printing of polysulfone and polyaniline composites, *Polymer* 152 (2018) 18–24.
- [22] B. Holmes, L.G. Zhang, Enhanced human bone marrow mesenchymal stem cell functions in 3D bioprinted biologically inspired osteochondral construct, *Proceedings of ASME* 2013, November 15–21, San Diego, USA (2013).
- [23] **Validating Isotropy in SLA 3D Printing**, [Online], 2017, Available: <https://formlabs.com/blog/isotropy-in-sla-3d-printing/> [August 1 September 2020].
- [24] R. Smerd, S. Winkler, C.P. Salisbury, M.J. Worswick, D. Lloyd, M. Finn, High strain rate tensile testing of automotive aluminum alloy sheet, *Int. J. Impact Eng.* 32 (1–4) (2005) 541–560.
- [25] A. Bardelcik, C.P. Salisbury, S. Winkler, M.A. Wells, M.J. Worswick, Effect of cooling rate on the high strain rate properties of boron steel, *Int. J. Impact Eng.* 37 (6) (2010) 694–702.
- [26] V.S. Deshpande, N.A. Fleck, M.F. Ashby, Effective properties of the octet-truss lattice material, *J. Mech. Phys. Solids* 49 (8) (2001) 1747–1769.
- [27] F. Huberth, S. Hiermaier, M. Neumann, Material models for polymers under crash loads existing LS-DYNA models and perspective, German LS-DYNA Forum, 2005 October 20–21, Bamberg, Germany (2005).
- [28] T. Erhart, Review of solid element formulations in LS-DYNA, German LS-DYNA Forum, October 12–13, Filderstadt, Germany (2011).
- [29] A.S. Hargreaves, The effect of the environment on the crack initiation toughness of dental poly(methyl methacrylate), *J. Biomed. Mater. Res.* 15 (1981) 757–768.
- [30] A.N. Ghebremeskel, C. Vemavarapu, M. Lodaya, Use of surfactants as plasticizers in preparing solid dispersions of poorly soluble API: selection of polymer-surfactant combinations using solubility parameters and testing the processability, *Int. J. Pharm.* 328 (2007) 119–129.
- [31] E.H. Andrews, G.M. Levy, J. Willis, Environmental crazing in a glassy polymer: the role of solvent absorption, *J. Mater. Sci.* 8 (1973) 1000–1008.
- [32] P. Wang, S. Lee, J.P. Harmon, Ethanol-induced crack healing in poly(methyl methacrylate), *J. Polym. Sci. Part B: Polym. Phys.* 32 (1994) 1217–1227.
- [33] D. Vlissidis, A. Prombonas, Effect of alcoholic drinks on surface quality and mechanical strength of denture base materials, *J. Biomed. Mater. Res.* 38 (3) (1997) 257–261.
- [34] C.B. Neves, L.P. Lopes, H.F. Ferrão, J.P. Miranda, M.F. Castro, A.F. Bettencourt, Ethanol postpolymerization treatment for improving the biocompatibility of acrylic relines resins, *Biomed. Res. Int.* 2013 (2013) 1–9.
- [35] S. Basavarajappa, L. Perea-Lowery, S. Aati, A.A.A. Al-Kheraif, R. Ramakrishnaiah, J.P. Matinlinna, P.K. Vallittu, The effect of ethanol on surface of semi-interpenetrating polymer network (IPN) polymer matrix of glass-fibre reinforced composite, *J. Mech. Behav. Biomed. Mater.* 98 (2019) 1–10.
- [36] A. White, D. Burns, T.W. Christensen, Effective terminal sterilization using supercritical carbon dioxide, *J. Biotechnol.* 123 (2006) 504–515.
- [37] C. Yavuz, S.N.B. Oliaei, B. Cetin, O. Yesil-Celiktas, Sterilization of PMMA microfluidic chips by various techniques and investigation of material characteristics, *J. Supercrit. Fluids* 107 (2016) 114–121.
- [38] T.J.A.G. Munker, S.E.C.M. van de Vijfeijken, C.S. Mulder, V. Vespasiano, A. G. Becking, C.J. Kleverlaan, Effects of sterilization on the mechanical properties of poly(methyl methacrylate) based personalized medical devices, *J. Mech. Behav. Biomed. Mater.* 81 (2018) 168–172.
- [39] L. Di Landro, G. Sala, D. Olivieri, Deformation mechanisms and energy absorption of polystyrene foams for protective helmets, *Polym. Test.* 21 (2002) 217–228.
- [40] C. Ling, J. Ivens, P. Cardiff, M.D. Gilchrist, Deformation response of EPS foam under combined compression-shear loading. Part I: experimental design and quasi-static tests, *Int. J. Mech. Sci.* 144 (2018) 480–489.